$[Mo_2(CN)_{11}]^{5-}$ A Detailed Description of Ligand-Field Spectra and Magnetic Properties by First-Principles Calculations

Marc F. A. Hendrickx,* S. Clima, L. F. Chibotaru, and A. Ceulemans

Katholieke Universiteit Leuven, Department of Chemistry, Celestijnenlaan 200F, B-3001 Leuven, Belgium

Received: February 22, 2005; In Final Form: July 11, 2005

An ab initio multiconfigurational approach has been used to calculate the ligand-field spectrum and magnetic properties of the title cyano-bridged dinuclear molybdenum complex. The rather large magnetic coupling parameter *J* for a single cyano bridge, as derived experimentally for this complex by susceptibility measurements, is confirmed to a high degree of accuracy by our CASPT2 calculations. Its electronic structure is rationalized in terms of spin−spin coupling between the two constituent hexacyano−monomolybdate complexes. An in-depth analysis on the basis of Anderson's kinetic exchange theory provides a qualitative picture of the calculated CASSCF antiferromagnetic ground-state eigenvector in the Mo dimer. Dynamic electron correlations as incorporated into our first-principles calculations by means of the CASPT2 method are essential to obtain quantitative agreement between theory and experiment.

1. Introduction

The synthesis of single-molecule magnets has become a widespread research topic in the past decade.[1] In this regard and also for the assembling of two- and three-dimensional magnetic solids, the monometalate cyanocomplexes appear to be excellent precursors. One major objective is to obtain magnetic ordering at high temperatures. First successes in this respect were obtained for the chromovanadium Prussian blue analogues.[2−5] Later studies demonstrated that the replacement of a first-row transition metal in this kind of compound for a second-row transition metal enhances the magnetic ordering temperature because of the stronger magnetic exchange coupling, which itself is a direct consequence of the more diffuse nature of the high-energy valence 4d orbitals.[6] Recently, several compounds with an octahedral hexacyanomolybdate as a building block have been synthesized.[6−8] One of the most interesting among them is the cyano-bridged $[Mo_2(CN)_{11}]^{5-}$ complex (**I**), for which the strongest exchange coupling through a single cyanide bridge has been measured: $J = -113$ cm^{-1}. The present contribution comprises a first-principles description of the electronic structure and the resulting magnetic properties of this dinuclear complex, as well as the computational results for the two distinct constituent hexacyanomolybdate complexes. One of these has all six cyanide ligands carbon-coordinated $[Mo(CN)_6]^{3-}$ (**II**), whereas the second one $[Mo(CN)_5(NC)]^{3-}$ (**III**) has the bridging cyanide ligand nitrogen-coordinated. A complete analysis of the electronic structure of the parent $[Mo(CN)_6]^{3-}$ has already been carried out by us.[9] In this paper, we will join these results with the ones newly obtained for the two building blocks of the $[Mo_2(CN)_{11}]^{5-}$ complex. This will form the basis for an in-depth analysis of the antiferromagnetic ground state of this dinuclear complex.

2. Computational Details

The electronic structures of complex **I**, as well as for the two building blocks **II** and **III**, have been studied by performing multireference ab initio calculations on their idealized structures, as they can be derived from the experimentally determined geometries.[7] In the $(Et_4N)_5[Mo_2(CN)_{11}]$ crystal, the dinuclear complex anion is observed to have almost a C_{4v} symmetry. Indeed, the differences in bond lengths between the equatorial (placed in the *x* and *y* directions as depicted in Figure 1) cyanide ligands are very small, differing by no more than 0.01 Å for the C−N and Mo−C bonds, while the bond angles deviate from the perfect point group symmetry by no more than 2.5°. All our calculations were carried out on geometries that were obtained by averaging the Mo−C and C−N equatorial bonds to 2.197 and 1.149 Å, respectively. The Mo−C and C−N distances of the axial ligands (placed on the *z* axis) were set equal to 2.176 and 1.149 Å for the two peripheral cyanides and to 2.125 and 1.187 Å for the bridging cyanide. According to the crystallographic data, the Mo−N bond distance for this ligand more or less equals the value of its Mo−C bond. All bond angles were fixed at either 90° or 180° as required for C_{4v} symmetry.

Extensive studies on the performance of the multiconfigurational second-order perturbation method (CASPT2) have shown that it is able to calculate accurate magnetic coupling parameters for a wide range of dinuclear complexes, organic biradicals, and transition metal-containing ionic insulators.[10,11] Also, its performance in calculating electronic spectra of the related $[Mo(CN)_6]^{3-}$, $[Mo(CN)_8]^{3-}$, and $[Mo(CN)_8]^{4-}$ transition metal complexes is sufficient to describe the ligand-field spectrum.[9,12−14] The calculations on compounds **II** and **III** have been performed by employing a minimal active space for the expansion of the zeroth-order CASSCF wave function. It comprises the five 4d molybdenum orbitals among which the three valence electrons are distributed: CAS(3,5). For the dinuclear complex **I**, two different complete active spaces have been used as a starting point for the CASPT2 calculations. The first is a minimal active space that consists of the ten 4d orbitals containing the six valence electrons of the two molybdenum(III) cations: CAS(6, 10). The second one is an extended active space that also includes along with the minimal active space the 5s, π, and π^* orbitals of the bridging cyanide ligand and its six valence electrons. This second active space can therefore

10.1021/jp0509257 CCC: $30.25
Published on Web 09/09/2005

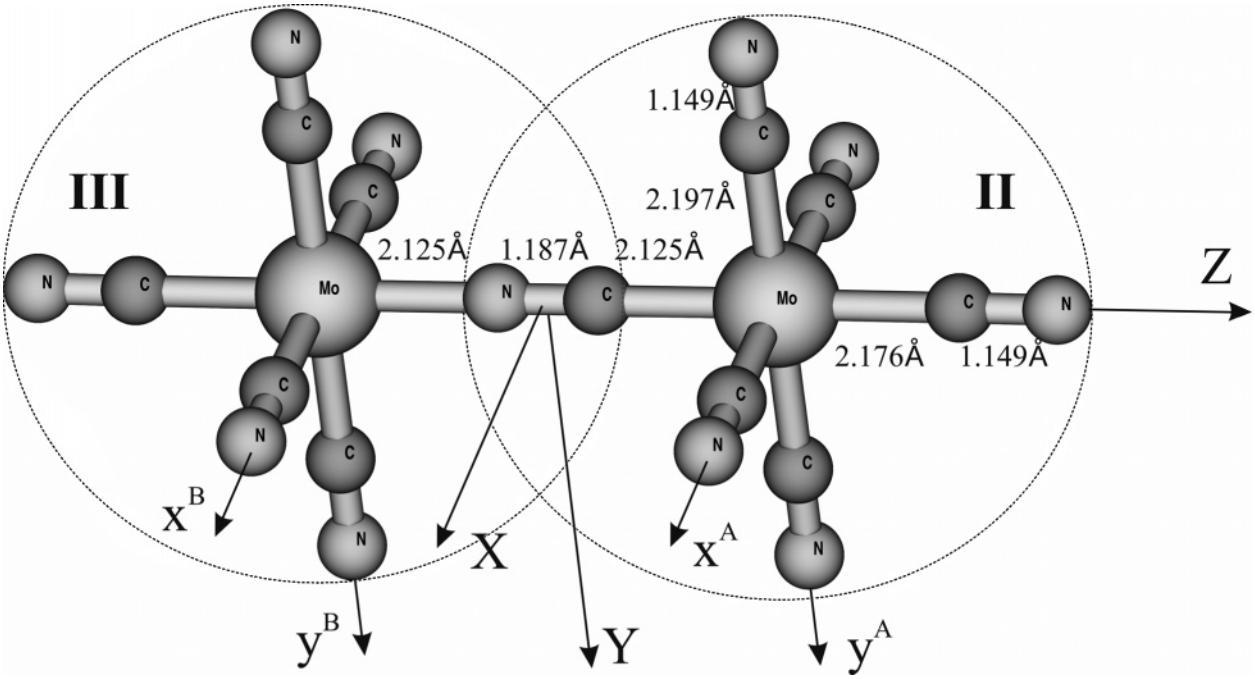

Figure 1. Structure of the dinuclear complex (**I**) and the two mononuclear complexes (**II**) and (**III**).

TABLE 1: Comparison of the CASPT2 Excitation Energies for the Ligand-Field Transitions of the Octahedral $[Mo(CN)_6]^{3-}$ (Ref 9) and the Two C_{4v} Fragments of the Dinuclear Complex I (this work)[a]

O_h state	$[Mo(CN)_6]^{3-}$ O_h (ref 9)	$[Mo(CN)_6]^{3-}$ C_{4v} (this work)	$[Mo(CN)_5(NC)]^{3-}$ C_{4v} (this work)	C_{4v} state
$^4A_{2g}(xy)^1(xz)^1(yz)^1$	0	0	0	$^4B_1$
^2E_g ($t_{2g} \rightarrow t_{2g}$)	9430	9480	10147	$^2A_1$ ($e \rightarrow e$)
		9971	10624	$^2B_1$ ($e \rightarrow e$)
$^2T_{1g}$ ($t_{2g} \rightarrow t_{2g}$)	9761	9590	10053	$^2A_2$ ($e \rightarrow e$)
		10114	10992	^2E ($e \rightarrow b_2$),($b_2 \rightarrow e$)
$^2T_{2g}$ ($t_{2g} \rightarrow t_{2g}$)	13924	13528	14915	$^2B_2$ ($e \rightarrow e$)
		13854	15389	^2E ($e \rightarrow b_2$),($b_2 \rightarrow e$)
$^4T_{2g}$ ($t_{2g} \rightarrow e_g$)	42647	41023	40532	$^4B_2$ ($b_2 \rightarrow b_1$)
		42791	38263	^4E ($e \rightarrow a_1$)
$^4T_{1g}$ ($t_{2g} \rightarrow e_g$)	45851	46099	43360	^4E ($e \rightarrow b_1$)
		47251	42819	$^4A_2$ ($b_2 \rightarrow a_1$)

[a] Excitation energies in wavenumbers (cm^{-1}).

be abbreviated as CAS(12,15). At the CASPT2 level, the dynamic correlation was calculated by including all the molecular orbitals of the complexes originating from all the valence atomic orbitals, i.e., the 2s and 2p orbitals of the carbon and nitrogen atoms and the 4p and 4d orbitals of molybdenum. For carbon and nitrogen [3s, 2p, 1d], one-electron basis sets of the ANO-S type as present in the library of the MOLCAS 6.0 software package[15] are used. The inner electrons for the molybdenum cations are replaced by relativistic effective core potentials, whereas the remaining 4p, 5s, and 4d valence orbitals are described by an (11s, 8p, 7d)/[3s, 3p, 4d] basis set.[15,16] For the dinuclear complex, we also employed the rather large all-electron (21s, 17p, 12d, 5f) /[8s, 7p, 5d, 2f] ANO-RCC basis set for the two transition metal centers.[15] In this case, the final CASPT2 total energies were obtained by taking into account scalar relativistic effects according to the Douglas−Kroll method,[17] as recommended by the authors of this basis set.[15]

3. Results and Discussion

3.1. Ligand-Field Spectra. For an understanding of the ligand-field spectra of the hexacoordinated complexes, it is particularly useful to have a close look at the metal−ligand bond distances. In comparison to the highly symmetric O_h $[Mo(CN)_6]^{3-}$ complex, as calculated by us previously,[9] the geometry of complex **II** differs in two aspects. First, the two axial Mo−C bonds of **II** are shorter. In particular, the Mo−C bond of 2.125 Å of the bridging cyanide ligand is substantially shorter than the O_h bond lengths of 2.181 Å, whereas the coordination bond of the other axial ligand at the opposite side of the complex is only slightly shorter (2.176 Å). This contraction of the axial axis is accompanied by a slight elongation of the equatorial Mo−C bonds to 2.197 Å. Exactly the same remarks can be made about the geometry of the $[Mo(CN)_5(NC)]^{3-}$ complex, as all the coordination bond lengths are the same, including the Mo−N bond of **III** when compared to the Mo−C bond of the bridging ligand in **II**.

The calculated transition energies for the lowest ligand-field states for complexes **II** and **III** are collected in Table 1 together with the results for the O_h complex of ref 9. The ground states for these d^3 complexes are all quartets possessing a $(d_{xy})^1$ $(d_{xz})^1$ $(d_{yz})^1$ configuration, which indicates a relatively small splitting of the d_π orbitals in the two C_{4v} complexes **II** and **III**. The same effect in combination with the half-filled shell nature accounts for the small splittings and shifts of the low-lying doublet states of complex **II** when compared with the O_h

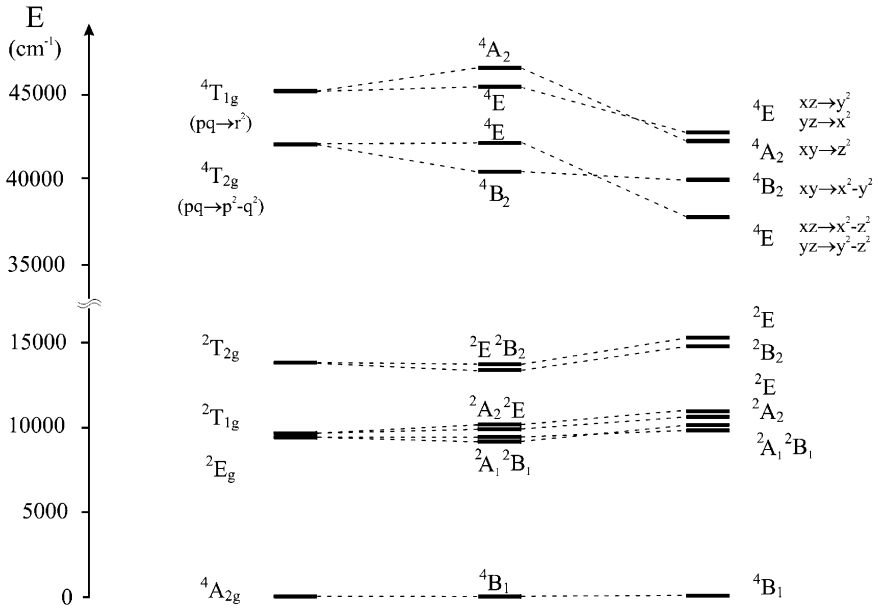

Figure 2. Energy level diagram for the mononuclear hexacyanocomplexes: left side, octahedral environment (ref 9); center, $[Mo(CN)_6]^{3-}$ complex (**II**) (present work); and right side, $[Mo(NC)(CN)_5]^{3-}$ complex (**III**) (present work).

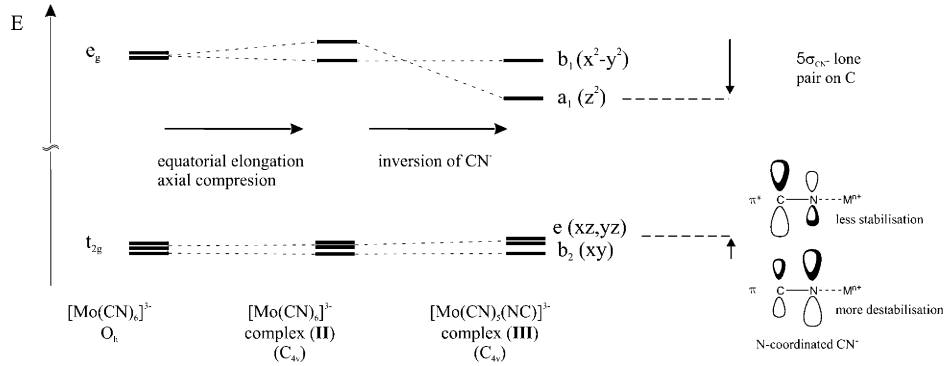

Figure 3. Qualitative orbital diagram of the Mo 4d orbitals in the octahedral hexacyanocomplex, the C_{4v} distored $[Mo(CN)_6]^{3-}$ (**II**), and $[Mo(CN)_5(NC)]^{3-}$ (**III**).

complex.[18] Indeed, these doublets all originate from the same octahedral $(t_{2g})^3$ configuration. The maximal splitting for the doublets of **II** occurs for $^2T_{1g}$ and amounts to 524 cm^{-1}. Also for complex **II** and as depicted in Figure 2, the energy splittings are more pronounced for the quartet excited states. This is a direct consequence of the excitation of an electron from a t_{2g} orbital to one of the e_g orbitals, which are destabilized by σ antibonding interactions with the ligand orbitals. For these quartet states $^4T_{2g}$ ($pq \rightarrow p^2 - q^2$) and $^4T_{1g}$ ($pq \rightarrow r^2$), the symmetry lowering induces gaps between ^4E, $^4B_2$ and ^4E, $^4A_2$ levels of 1768 and 1152 cm^{-1}, respectively. The $^4B_2$ ($xy \rightarrow x^2 - y^2$) component of the octahedral $^4T_{2g}$ state is situated below the corresponding ^4E ($xz \rightarrow x^2 - z^2$, $yz \rightarrow y^2 - z^2$) state, while the $^4A_2$ ($xy \rightarrow z^2$) component of $^4T_{1g}$ is positioned above the corresponding ^4E ($xz \rightarrow y^2$, $yz \rightarrow x^2$). The origin of this ordering is the result of the equatorial elongation of the Mo−C bonds in complex **II** that stabilizes $d_{x^2-y^2}$ and a simultaneous stronger axial compression by which d_{z^2} is strongly destabilized. As a consequence, the transition to the $^4B_1$ excited state is shifted downward for 1624 cm^{-1}, whereas the ^4E transition occurs at slightly higher energies (+144 cm^{-1}) than the octahedral $^4T_{2g}$ transition. In comparison with the excitation energy for $^4T_{1g}$ of the O_h complex, the same line of reasoning explains the higher excitation energy calculated for $^4A_2$ (+1400 cm^{-1}) and the hardly affected relative position of the corresponding ^4E state (+248 cm^{-1}).

The other constituent part of the dinuclear complex at hand, complex **III** of Figure 1, exclusively differs from **II** in the fact that one cyanide ligand is nitrogen-coordinated rather than carbon-coordinated. In this case, we can expect an even stronger axial distortion from the octahedral symmetry. Since the HOMO 5σ orbital of cyanide is in essence an sp lone-pair orbital on carbon, d_{z^2} of $[Mo(CN)_5(NC)]^{3-}$ is especially lowered because of smaller σ antibonding interactions with nitrogen. On the other hand, the stronger π antibonding interactions with the occupied π orbitals of this cyanide ligand (main contribution on the more electronegative N) and the smaller bonding interactions with the unoccupied π^* orbitals raise the energies of the d_{xz} and d_{yz} orbitals with respect to d_{xy}. Figure 3 depicts a summary of these qualitative orbital considerations. On the basis of this simple orbital picture, we can conclude that the relative positions of the d_{xy} and $d_{x^2-y^2}$ orbitals are unchanged by the inversion of an axial cyanide ligand. Therefore, the excitation energies in Table 1 for the $^4B_1 \rightarrow {}^4B_2$ ($xy \rightarrow x^2 - y^2$) transitions are nearly the same in **II** and **III**. All the other quartet transitions are to be found at lower energies in **III** than in **II**. The lower energy of the $^4A_2$ ($xy \rightarrow z^2$) state is solely due to the smaller antibonding effects in the d_{z^2} orbital of **III**. The lower transition energies

TABLE 2: Ligand-Field Transitions of $[Mo_2(CN)_{11}]^{5-}$: Effective Core Potential (ECP) and All-Electron (AE) CASPT2 Excitation Energies obtained for the (6, 10) and (12, 15) Active Spaces[a]

C_{2v} state	(6, 10) ECP	(12, 15) ECP	(6, 10) AE	(12, 15) AE
$^1A_1$	0	0	0	0
$^3A_1$	193	216	208	208
$^5A_1$	668	625	569	594
$^7A_1$	959	1186	1077	1110
$^3A_2$	10754	10682	10019	9054
$^5A_2$	10731	10411	9894	9214
$^5B_{1,2}$	11416	11314	11213	9728
$^3B_{1,2}$	10882	10508	10636	9729
$^1B_{1,2}$	20262	19439	18808	17052
$^1A_2$	20167	19311	18041	17133
$^7B_{1,2}$	40181	40542	41167	35923
$^7A_2$	42162	42786	43562	41053

[a] States classified according to the C_{2v} point group and transition energies in wavenumbers (cm^{-1}).

for the two ^4E states ($xz \rightarrow y^2$, $yz \rightarrow x^2$, or $xz \rightarrow x^2 - z^2$, $yz \rightarrow y^2 - z^2$) are the result of the combined effects of the destabilization of the d_π orbitals and the stabilization of the d_σ-type orbitals. In comparison to **II** and without any exception, all the doublet transitions in Table 1 are located at higher energies in **III**. Most likely, the reduced π back-bonding in **III** lies at the origin of the smaller nephelauxetic reduction in this hexacyanocomplex.[19]

Despite the differences between the spectra of **II** and **III** as discussed in the previous paragraph, there is an overall good resemblance between them. Doublet states are situated at about 10 000 cm^{-1}, and excited quartet states are positioned around 40 000 cm^{-1}. Deviations between the two spectra amount to a few thousand wavenumbers. The calculated CASPT2 transition energies for some low-lying electronic states of the dinuclear complex **I**, classified according to the C_{2v} point group, are collected in Table 2. The second and third columns of this table contain the results of the calculations performed with the effective core description for the two molybdenum centers. The excitation energies for the minimal (6, 10) active space (4d orbitals of Mo) and the larger (12, 15) active space can be found in the second and third column, respectively. The fourth and fifth columns of the same table contain the results obtained for the same active spaces in combination with the all-electron basis set. A first inspection of Table 2 allows us to conclude that the deviations between the various computational models are most probably smaller than the expected accuracy of the computations. Indeed, the well-known accuracy of the CASPT2 method for ligand-field transition energies is about 2000 wavenumbers.[9,12−14] Therefore, in the following discussion of the ligand-field spectrum of complex **I**, we shall make use of the values obtained for the larger active space (12, 15) and the all-electron basis set (last column of Table 2). As a first approximation, we can consider the two metal centers as weakly coupled, which implies that the resulting spectrum of the dinuclear complex can be derived in a simple way from the individual spectra of the two constituent hexacyanocomplexes as described in previous paragraphs. As will be demonstrated in detail in the following section, the lowest singlet and septet states are indeed in zeroth-order approximation the outcome of an exchange coupling of the two $^4B_1$ ground states of complexes **II** and **III**. According to Table 2, this coupling can also give rise to a low-lying triplet, quintet, and septet. All these states possess an A_1 symmetry. The exchange interactions result in an antiferromagnetic low-spin $^1A_1$ ground state for **I**, which is positioned at 1110 cm^{-1} below the high-spin $^7A_1$ state. Between and in increasing energies lie the $^3A_1$ and $^5A_1$ states at 208 and 594 cm^{-1}, respectively. Further, a weak exchange coupling between the $^4B_1$ ground state of one metal center with a doublet of the other center predicts triplet and quintet states with energies relative to the ground state of about 10 000 cm^{-1}, i.e., the average excitation energy of doublets in the two hexacyanocomplexes. Indeed, Table 2 shows that the CASPT2 method calculates several such states in this energy region, for example $^3A_2$, $^3B_{1,2}$, $^5A_2$, and $^5B_{1,2}$ at 9054 cm^{-1}, 9729, 9728, and 9214 cm^{-1}, respectively. Beside the low-spin ground state, several other singlet states are to be expected as the result of exchange coupling between two doublet states of **II** and **III**. A weak interaction implies excitation energies that are twice as large as those calculated for the triplets and quintets, e.g., $^1B_{1,2}$ (17 052 cm^{-1}) and $^1A_2$ (17 133 cm^{-1}). Finally, low-lying septet states of **I** will be the result of an interaction between a quartet excited state of one metal center with the ground state of the other metal site and predicted at the excitation energies of these quartets in the mononuclear complexes **II** and **III**. Two examples are given in Table 2, namely $^7B_1$ (35 923 cm^{-1}) and $^7A_2$ (41 053 cm^{-1}). For the sake of completeness, it should be mentioned that charge-transfer transitions are expected to occur at excitation energies smaller than these values. Indeed, in the octahedral $[Mo(CN)_6]^{3-}$ complex, ligand-to-metal charge-transfer (LMCT) transitions are calculated at about 30 000 cm^{-1}.[9] All the theoretical findings mentioned so far explain satisfactorily the experimental spectrum of the dinuclear complex **I**.[7] The low-intensity and low-energy transitions that are recorded between 10 000 and 20 000 cm^{-1} are predicted to be ligand-field transitions, while the high-intensity and high-energy bands in the experimental spectrum should be ascribed to LMCT transitions. Our calculations predict no metal-to-metal transitions below 40 000 cm^{-1}. In summary, it follows from our CASPT2 treatment that the general features of the electronic spectrum of the dinuclear complex can, in broad terms, easily be derived from the spectra of the two independent constituent hexacyanocomplexes. For the finer details of the electronic effects that are responsible for the experimental observed splittings between the lowest magnetic states, a more elaborated analysis of the wave functions is needed.

3.2. Magnetic Properties.

3.2.1. Magnetic Spectrum. From an analysis of the CASPT2 energies, it turned out that the spectrum of the lowest-spin multiplets of the dimer **I** is adequately described by the Heisenberg Hamiltonian

$$\hat{H} = -2J\hat{S}_{Mo(1)}\hat{S}_{Mo(2)} \quad (1)$$

including spin operators of the molybdenum sites and the exchange parameter. For the specific example at hand, the antiferromagnetic contribution to the latter is given by Anderson's kinetic exchange theory as follows:[21]

$$J = -\frac{4t_e^{\,2}}{9U} \quad (2)$$

Here, the parameter t_e is the hopping parameter, defined as the exchange matrix element between two d_π orbitals that show positive overlap. The parameter U denotes the Coulomb repulsion due to the transfer of one electron to a different center, taken as the same for both transfer directions. Using the (12, 15) active space and the all-electron basis set CASSCF places the $^3A_1$, $^5A_1$, and $^7A_1$ states at 78, 229, and 442 cm^{-1} above the ground state, respectively. These energies can be fitted to eq 1 quite well with a J value of approximately -38 cm^{-1}. By fitting the temperature dependence of the magnetic susceptibility to

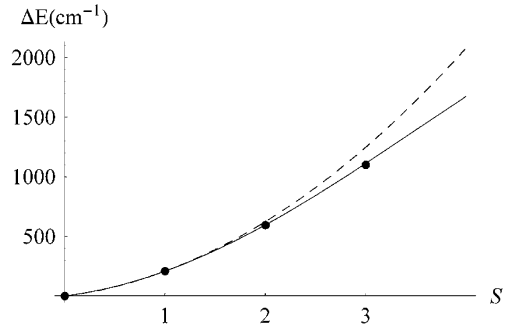

Figure 4. Landé interval fitting by using eq 1 (dashed line) and by including the biquadratic term as in eq 3 (continuous line).

the Hamiltonian (eq 1), Long et al.[7] arrived at an experimental exchange interaction parameter J of -113 cm^{-1} that deviates much from our CASSCF estimate. Hence, the incorporation of dynamic correlation by means of, for instance, CASPT2 is an absolute necessity in order to reach an acceptable quantitative agreement between theory and experiment.[22−25]

As stated earlier, the $[Mo_2(CN)_{11}]^{5-}$ (**I**) dinuclear cyanide compound exhibits the strongest antiferromagnetic coupling through a single cyanide bridge measured so far. The experimental J value of -113 cm^{-1} implies an energy splitting between the singlet ground state and the first excited triplet state of 226 cm^{-1}, which is close to our CASPT2 calculated value of 208 cm^{-1} (Table 2). Our best theoretical J value, as obtained with the largest active space and basis set, is, therefore, only slightly different: -104 cm^{-1}. For the higher-lying $^5A_1$ and $^7A_1$ magnetic states, the deviation between the Heisenberg model and the calculated excitation energies become increasingly larger (Figure 4). Indeed, on the basis of the Heisenberg Hamiltonian, Landé-type interval gaps are expected, which puts the quintet and septet states at 624 (678) cm^{-1} and 1248 (1356) cm^{-1}, where the numbers in brackets refer to the experimental J value. In particular for the septet, the difference between the CASPT2 excitation energy (1110 cm^{-1}) and the Heisenberg energy as calculated with the experimental J value (1356 cm^{-1}) is quite large, while the theoretical value for J reduces the difference by about one-half. Clearly, the energies of the higher-spin multiplets $^5A_1$ and $^7A_1$ cannot be derived with high accuracy from fitting the susceptibility curve in the temperature region up to 300 K. On the other hand, the CASPT2 results indicate that corrections to the Heisenberg model should be included in order to reproduce the spectrum of calculated spin levels. In the absence of spin−orbit coupling effects, the total spin of the complex is always a good quantum number.[26] Therefore, the lowest-order correction to the spin Hamiltonian (eq 1) preserving the total spin is of the form $\sim(\hat{S}_1\cdot\hat{S}_2)^2$, giving rise to the biquadratic exchange interaction

$$\hat{H} = -2J\hat{S}_1\hat{S}_2 + j(\hat{S}_1\hat{S}_2)^2 \qquad (3)$$

By using the expression $\hat{S}^2 = \hat{S}_1^2 + 2\hat{S}_1\hat{S}_2 + \hat{S}_2^2$ and a least-squares fitting procedure, the eigenvalues of the Hamiltonian (eq 3) were found to be in excellent agreement with the lowest CASPT2 spin multiplets for $J = -89$ cm^{-1} and $j = -4.5$ cm^{-1}. The latter value indicates significant deviation from the Heisenberg Hamiltonian (eq 1) and is additional evidence for a strong mixing of the magnetic orbitals. The obtained strong deviations from the Landé intervals rule in the low-lying spectrum of the spin states could be checked by performing inelastic neutron scattering experiments for this compound.[27]

3.2.2. The Antiferromagnetic Ground State. In this paragraph, we will demonstrate how the calculated CASSCF wave function

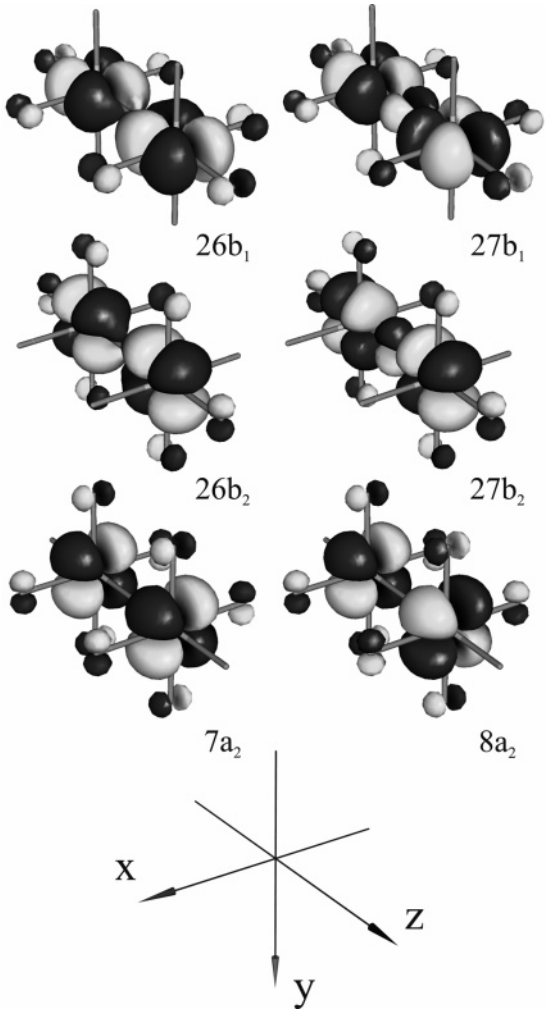

Figure 5. Active molecular orbitals of the $[Mo_2(CN)_{11}]^{5-}$ dinuclear complex. Per irreducible representation, each couple of molecular orbitals shows an in-phase and out-of-phase combination of the metal 4d atomic orbitals on each metal center.

of the singlet ground state for $[Mo_2(CN)_{11}]^{5-}$ can be derived to a very large degree from the coupling of the usual $(t_{2g})^3$ quartet ground states of its two magnetic Mo^{3+} centers when corrected to first order for the kinetic exchange effects. The spin components of the ground wave vector on, say, magnetic center A can be written in determinantal form as

$$|^4A_{2g}, +^3/_2\rangle = |d^A_{xz}\alpha d^A_{yz}\alpha d^A_{xy}\alpha|$$

$$|^4A_{2g}, +^1/_2\rangle = \frac{1}{\sqrt{3}}(|d^A_{xz}\alpha d^A_{yz}\alpha d^A_{xy}\beta| + |d^A_{xz}\alpha d^A_{yz}\beta d^A_{xy}\alpha| + |d^A_{xz}\beta d^A_{yz}\alpha d^A_{xy}\alpha|)$$

$$|^4A_{2g}, -^1/_2\rangle = \frac{1}{\sqrt{3}}(|d^A_{xz}\beta d^A_{yz}\beta d^A_{xy}\alpha| + |d^A_{xz}\beta d^A_{yz}\alpha d^A_{xy}\beta| + |d^A_{xz}\alpha d^A_{yz}\beta d^A_{xy}\beta|)$$

$$|^4A_{2g}, -^3/_2\rangle = |d^A_{xz}\beta d^A_{yz}\beta d^A_{xy}\beta| \qquad (4)$$

where we adopt the standard dimer frame of the ab initio calculation, with the origin in the middle of the central cyanide bridge and the z-axis along the bridge oriented from N to C (Figure 1). On each Mo, we further define a local xyz frame, which is parallel to the main XYZ frame. Hence, the local frames

are obtained by *translations* of the main frame along the positive or negative *z*-axis. The frame on Mo along the positive *z*-axis is labeled $x^A y^A z^A$, and similarly with *B* for the frame on Mo along the negative *z*-axis. A notation such as d^A_{xz} refers to a d_{xz} orbital on center *A* with the standard orientation in the local Cartesian frame.

The metal contributions to the active molecular orbitals (MOs) that are depicted in Figure 5, can now be expressed as sums and differences of the local t_{2g} functions.

$$|26b_1\rangle = \frac{1}{\sqrt{2}}(d^A_{xz} + d^B_{xz})$$

$$|27b_1\rangle = \frac{1}{\sqrt{2}}(-d^A_{xz} + d^B_{xz})$$

$$|26b_2\rangle = \frac{1}{\sqrt{2}}(-d^A_{yz} - d^B_{yz})$$

$$|27b_2\rangle = \frac{1}{\sqrt{2}}(-d^A_{yz} + d^B_{yz})$$

$$|7a_2\rangle = \frac{1}{\sqrt{2}}(-d^A_{xy} - d^B_{xy})$$

$$|8a_2\rangle = \frac{1}{\sqrt{2}}(d^A_{xy} - d^B_{xy}) \qquad (5)$$

In the combinations $26b_1$ and $26b_2$ with a central nodal plane, delocalization is via the π^* orbitals of the bridging cyanide, which clearly show back-bonding to the metal orbitals. In the alternate combinations, $27b_1$ and $27b_2$, the bridging is via the central cyanide π orbitals. Clearly in these cases, the interaction between the central ligand and the metal d_π orbitals is antibonding, as required by the π-donor character of these ligand-field interactions. From these equations, we can also obtain the inverse transformation, which expresses the magnetic orbitals in the MO basis, i.e.,

$$d^A_{xz} = \frac{1}{\sqrt{2}}(|26b_1\rangle - |27b_1\rangle)$$

$$d^B_{xz} = \frac{1}{\sqrt{2}}(|26b_1\rangle + |27b_1\rangle)$$

$$d^A_{yz} = \frac{1}{\sqrt{2}}(-|26b_2\rangle - |27b_2\rangle)$$

$$d^B_{yz} = \frac{1}{\sqrt{2}}(-|26b_2\rangle + |27b_2\rangle)$$

$$d^A_{xy} = \frac{1}{\sqrt{2}}(-|7a_2\rangle + |8a_2\rangle)$$

$$d^B_{xy} = \frac{1}{\sqrt{2}}(-|7a_2\rangle - |8a_2\rangle) \qquad (6)$$

Next, we derive—always within the d-only approach—the zeroth-order wave function for the singlet ground state. The coupling of the two fragment quartets to a resulting dimer singlet follows the usual vector addition scheme, as can be found, for instance, in Appendix 6 to Kahn's book.[20] One has

$$\Psi_0 = \frac{1}{2}(|^3/_2, -^3/_2\rangle - |^1/_2, -^1/_2\rangle + |-^1/_2, {}^1/_2\rangle - |-^3/_2, {}^3/_2\rangle) \qquad (7)$$

TABLE 3: Analysis of the CASSCF $^1A_1$ Wave Function in Terms Zeroth-Order Contribution Ψ_0 and First-Order Kinetic Exchange Contribution Ψ_1

	CSF	Ψ_0	Ψ_1	Ψ	CASSCF
ϕ_1	20 20 20	−0.250	+0.433	−0.281	−0.28536
ϕ_2	20 02 20	+0.250	0	+0.250	+0.24870
ϕ_3	20 20 02	+0.250	−0.433	+0.281	+0.28516
ϕ_4	20 02 02	−0.250	0	−0.250	−0.24855
ϕ_5	02 20 20	+0.250	0	+0.250	+0.24870
ϕ_6	02 02 20	−0.250	−0.433	−0.219	−0.22290
ϕ_7	02 20 02	−0.250	0	−0.250	−0.24855
ϕ_8	02 02 02	+0.250	+0.433	+0.219	+0.22280
χ_1	20 uu dd	+0.2887	−0.250	+0.307	+0.30442
χ_2	uu dd 20	+0.2887	0	+0.289	+0.28337
χ_3	uu 20 dd	−0.2887	+0.250	−0.307	−0.30442
χ_4	uu 02 dd	+0.2887	+0.250	+0.271	+0.26904
χ_5	uu dd 02	−0.2887	0	−0.289	−0.28320
χ_6	02 uu dd	−0.2887	−0.250	−0.271	−0.26904

Here, the components are $|M_S, M'_S\rangle$ states where M_S refers to the spin component on *A* and M'_S to the spin component on *B*. When the product is formed, the two three-electron determinants are fused to a single six-electron determinant, with full antisymmetrization, e.g.,

$$|^3/_2, -^3/_2\rangle = |d^A_{xz}\alpha d^A_{yz}\alpha d^A_{xy}\alpha d^B_{xz}\beta d^B_{yz}\beta d^B_{xy}\beta| \qquad (8)$$

A state such as $|^1/_2, -^1/_2\rangle$ is thus composed of 9 six-electron determinants. The wave vector in total has 20 components over the $(t_{2g})^3 - (t_{2g})^3$ configuration. To match this wave function with the CASSCF results, we must convert the local t_{2g}-orbitals into the delocalized molecular orbitals, using the expressions in eq 6. After a series of tedious substitutions, involving eqs 4, 6, and 7, one finds that Ψ_0 is composed of some 44 determinants over the 6 MO functions. Adopting the notations of the MOLCAS output, the spin-adapted configuration state functions (CSF) are written as a series of occupation numbers for the orbitals ordered as $26b_1$, $27b_1$, $26b_2$, $27b_2$, $7a_2$ and $8a_2$. For doubly occupied orbitals, say $(26b_1)^2$, the order of the spin−orbitals is taken as $26b_1\alpha 26b_1\beta$. For singly occupied orbitals, we specify the spin as u or d, for up (α) or down (β), respectively. Only two types of CSFs appear to be present, either with 3 doubly occupied orbitals of each irreducible representation or with 1 orbital doubly occupied and the 4 orbitals of the other representations all singly occupied. For the latter class, the open-shell orbitals are always coupled in an identical way, so the use of a compound symbol is in order. The following notation for these CSFs is taken from MOLCAS

$$\begin{aligned}(20)(uu)(dd) = \frac{1}{\sqrt{12}}(&-2|26b_1\alpha 26b_1\beta 26b_2\alpha 27b_2\alpha 7a_2\beta 8a_2\beta| \\ &-2|26b_1\alpha 26b_1\beta 26b_2\beta 27b_2\beta 7a_2\alpha 8a_2\alpha| \\ &+|26b_1\alpha 26b_1\beta 26b_2\alpha 27b_2\beta 7a_2\alpha 8a_2\beta| \\ &+|26b_1\alpha 26b_1\beta 26b_2\alpha 27b_2\beta 7a_2\beta 8a_2\alpha| \\ &+|26b_1\alpha 26b_1\beta 26b_2\beta 27b_2\alpha 7a_2\alpha 8a_2\beta| \\ &+|26b_1\alpha 26b_1\beta 26b_2\beta 27b_2\alpha 7a_2\beta 8a_2\alpha|)\end{aligned} \qquad (9)$$

The resulting zeroth-order vector is listed in the Table 3 together with the CASSCF wave function. The symmetry coefficients are seen to be already quite close to the CASSCF result, and all signs are consistent. Most importantly, the determinants which we have found account for almost 100% of the calculated

ground state, indicating that there is almost no admixture of excited configurations.

When the exchange interaction between the two metal centers is turned on, hopping between the centers will, according to Anderson's kinetic exchange theory,[21] perturb the symmetric zero-order results. We can model this interaction by a introducing a transfer term of the following type:

$$\hat{V} = -t_e \sum_{\sigma=\alpha,\beta} (a^{\dagger}_{xz\sigma} b_{xz\sigma} + a^{\dagger}_{yz\sigma} b_{yz\sigma} + b^{\dagger}_{xz\sigma} a_{xz\sigma} + b^{\dagger}_{yz\sigma} a_{xz\sigma}) \quad (10)$$

where $b_{xz\sigma}$ annihilates an electron with σ spin in d^B_{xz} and $a^{\dagger}_{xz\sigma}$ creates an electron with σ spin in d^A_{xz}. Note that the exchange interaction between d^A_{xy} and d^B_{xy} is neglected because of the very weak through-space δ overlap, as is evident from the virtually identical occupation of the $7a_2$ and $8a_2$ orbitals.

The operator $\hat{V}$ can be applied to the MOs using the expressions in eq 5. One obtains

$$\hat{V}|26b_1\rangle = \frac{1}{\sqrt{2}}(-t_e d^B_{xz} - t_e d^A_{xz}) = -t_e|26b_1\rangle$$

$$\hat{V}|26b_2\rangle = -t_e|26b_2\rangle$$

$$\hat{V}|27b_2\rangle = +t_e|27b_2\rangle$$

$$\hat{V}|7a_2\rangle = 0$$

$$\hat{V}|8a_2\rangle = 0 \quad (11)$$

We thus see that the gap between the in- and out-of-phase combinations of the d_π MOs equals $2t_e$. Since the out-of-phase combination is lower in energy, t_e is expected to be positive in this case. This coupling is due to through-bond interactions through the cyanide bridge.

Armed with these expressions, we can act with the $\hat{V}$ operator on Ψ_0. In this way, we obtain the $(t_{2g})^4 - (t_{2g})^2$ excited-state wave vector, Ψ_1, which provides a first-order correction to the wave vector.

$$\Psi_1 \approx \hat{V}\Psi_0 \quad (12)$$

The properly normalized vector expressed through the ϕ and χ determinantal combinations from the table reads

$$\Psi_1 = \frac{\sqrt{3}}{4}(\phi_1 - \phi_3 - \phi_6 + \phi_8) - \frac{1}{4}(\chi_1 - \chi_3 - \chi_4 + \chi_6) \quad (13)$$

To first order, the resulting wave vector is expressed as

$$\Psi = \Psi_0 - \frac{\langle\Psi_1|\hat{V}|\Psi_0\rangle}{E_1 - E_0}\Psi_1 \quad (14)$$

with

$$\frac{\langle\Psi_1|\hat{V}|\Psi_0\rangle}{E_1 - E_0} = \frac{4t_e}{\sqrt{3}U} \quad (15)$$

The overlap between the CASSCF wave function and Ψ_1 amounts to -0.0717. From this result, we finally obtain

$$\frac{t_e}{U} = 0.031 \quad (16)$$

As expected, the hopping parameter t_e is found to be positive. In Table 3, we have calculated the corrected wave function using eq 14. This is to be compared with the computed wave vector in the final column of the table. As can be seen, the agreement is quite good, which justifies the picture of localized magnetic electrons on the metal sites.

4. Conclusions

An analysis of the electronic structure of the two constituent mononuclear complexes, i.e., $[Mo(CN)_6]^{3-}$ and $[Mo(CN)_5(NC)]^{3-}$, by means of their calculated ligand-field spectra reveals only small differences between these two building blocks. In particular for the t_{2g} shells, the inversion of one cyanide ligand was found only to slightly change the relative energetic positions of the doublet excited states with respect to the quartet ground state. On this basis and by using Anderson's kinetic exchange theory, a detailed analysis of the CASSCF antiferromagnetic ground-state wave function of the dinuclear complex is given. Our present CASPT2 calculations confirm the high value of J for the dinuclear $[Mo_2(CN)_{11}]^{5-}$ complex as a measure for the splitting between the two lowest states. Including the quintet and septet magnetic states requires a somewhat smaller J value and the extension of the Heisenberg Hamiltonian with a biquadratic term.

Acknowledgment. Financial support by the Belgian National Science Foundation and the Flemish Government under the Concerted Action Scheme are gratefully acknowledged.

References and Notes

(1) Sessoli, R.; Gatteschi, D.; Caneschi, A.; Novak, M. *Nature (London)* **1993**, *365*, 141. Awschalom, D. D.; Di Vincenzo, D. P. *Phys. Today* **1995**, *48*, 43. Dahlberg, E. D.; Zhu, J.-G. *Phys. Today* **1995**, *48*, 34. Aubin, S. M. J.; Sun, Z. M.; Eppley, H. J.; Rumberger, E. M.; Guzei, I. A.; Folting, K.; Gantzel, P. K.; Rheingold, A. L.; Christou, G.; Hendrickson, D. N. *Inorg. Chem.* **2001**, *40*, 2127. Larionova, J.; Kahn, O.; Gohlen, S.; Ouahab, L.; Clerac, R. *J. Am. Chem. Soc.* **1999**, *121*, 3349. Ksenofontov, V.; Levchenko, G.; Reiman, S.; Gütlich, P.; Bleuzen, A.; Escax, V.; Verdaguer, M. *Phys. Rev. B* **2003**, *68*, 024415. Berseth, P. A.; Sokol, J. J.; Shores, M. P.; Heinrich, J. L.; Long, J. R. *J. Am. Chem.* Soc. **2000**, *122*, 9655. Batten, S. R.; Robson, R. *Angew. Chem., Int. Ed.* **1998**, *37*, 1460. Zhong, Z. J.; Seino, H.; Mizobe, Y.; Hidai, M.; Fujishima, A.; Ohkoshi, S.; Hashimoto, K. *J. Am. Chem. Soc.* **2000**, *122*, 2952.

(2) Holmes, S. M.; Girolami, G. S. *J. Am. Chem. Soc.* **1999**, *121*, 5593.

(3) Ferlay, S.; Mallah, T.; Ouahès, R.; Veillet, P.; Verdaguer, M. *Nature (London)* **1995**, *378*, 701.

(4) Sato, O.; Iyoda, T.; Fujushima, A.; Hashimoto, K. *Science* **1996**, *271*, 49.

(5) Buschmann, W. E.; Paulson, S. C.; Wynn, C. M.; Girtu, M. A.; Epstein, A. J.; White, H. S.; Miller, J. S. *Adv. Mater.* **1997**, *9*, 645.

(6) Shores, M. P.; Sokol, J. J.; Long, J. R. *J. Am. Chem. Soc.* **2002**, *124*, 2279.

(7) Beauvais, L. G.; Long, J. R. *J. Am. Chem. Soc*. **2002**, *124*, 2110.

(8) Sokol, J. J.; Hee, A. G.; Long, J. R. *J. Am. Chem. Soc.* **2002**, *124*, 7656.

(9) Hendrickx, M. F. A.; Mironov, V. S.; Chibotaru, L. F.; Ceulemans, A. *J. Am. Chem. Soc.* **2003**, *125*, 3694.

(10) de Graaf, C.; Sousa, C.; Moreira, I. D. R.; Illas, F. *J. Phys. Chem. A* **2001**, *105*, 11371.

(11) Queralt, N.; deGraaf, C.; Cabrero, J.; Caballol, R. *Mol. Phys.* **2003**, *101*, 2095.

(12) Pierloot, K.; VanPraet, E.; Vanquickenbourne, L. G. *J. Phys. Chem.* **1997**, *97*, 12220.

(13) Hendrickx, M. F. A.; Chibotaru, L. F.; Ceulemans, A. *Inorg. Chem.* **2003**, *42*, 590.

(14) Hendrickx, M. F. A.; Mironov, V. S.; Chibotaru, L. F.; Ceulemans, A. *Inorg. Chem.* **2004**, *43*, 3142.

(15) Karlström, G.; Lindh, R.; Malmqvist, P.-Å.; Roos, B. O.; Ryde, U.; Veryazov, V.; Widmark, P.-O.; Cossi, M.; Schimmelpfennig, B.; Neogrady, P.; Seijo, L. MOLCAS, version 6.0. *Comput. Mater. Sci.* **2003**, *28*, 222.

(16) Barandiaran, Z.; Seijo, L.; Huzinaga, S. *J. Chem. Phys.* **1990**, *93*, 5843.

(17) Douglas, N.; Kroll. N. M. *Ann. Phys.* **1974**, *82*, 89.

(18) Ceulemans, A. *Top. Curr. Chem.* **1994**, *171*, 27.

(19) Jorgensen, C. K. *Modern Aspects of Ligand Field Theory*; North-Holland Publishing Co.: Amsterdam, 1971.
(20) Kahn, O. *Molecular Magnetism*; VCH: New York, 1993.
(21) Anderson, P. W. *Phys. Rev* **1959**, *115*, 2. Anderson, P. W. *Solid State Physics*; Academic Press: London, 1963; Vol. 14.
(22) Calzado, C. J.; Cabrero, J.; Malrieu, J.-P.; Caballol, R. *J. Chem. Phys.* **2002**, *116*, 2728; 3985.
(23) Cabrero, J.; Calzado, C. J.; Maynau, D.; Caballol, R.; Malrieu, J.-P. *J. Phys. Chem. A* **2002**, *106*, 8146.
(24) van Oosten, A. B.; Broer, R.; Nieuwpoort, W. C. *Chem. Phys. Lett*. **1996**, *257*, 207.
(25) Broer, R.; Hozoi, L.; Nieuwpoort, W. C. *Mol. Phys*. **2003**, *101*, 233.
(26) Landau, L. D.; Lifshitz, E. M. *Quantum Mechanics*, 2nd ed.; Pergamon: Oxford, 1975.
(27) Güdel, H. U. In *Magneto-Strucutral Correlations in Exchange Coupling Systems*; Willet, R. D., Gatteschi, D., Kahn, O., Eds.; NATO ASI Series; Reidel: Dordrecht, 1985.